Structures and Buildings

ice Publishing

Fire resistance of bi-directionally prestressed concrete under extreme fire loading

Ji-Hun Choi PhD
Research Fellow, School of Civil and Environmental Engineering,
Yonsei University, Seoul, South Korea (Orcid:0000-0002-8079-2356)

Dal-Hun Yang PhD (DEng)
Postdoctoral Researcher, Department of Structural Engineering Research,
Korea Institute of Civil Engineering and Building Technology, Gyeonggi,
South Korea (Orcid:0000-0002-3996-7126)

Seung-Jai Choi PhD (DEng)
Postdoctoral Researcher, School of Civil and Environmental Engineering,
Yonsei University, Seoul, South Korea (Orcid:0000-0002-5456-8617)

Seong-Tae Yi PhD
Professor, Department of Civil and Environmental Engineering,
Inha Technical College, Incheon, South Korea
(Orcid:0000-0003-0907-7357)

Jang-Ho Jay Kim PhD
Professor, School of Civil and Environmental Engineering, Yonsei University,
Seoul, South Korea (Orcid:0000-0002-5138-8282)
(corresponding author: jjhkim@yonsei.ac.kr)

Infrastructures such as prestressed concrete containment vessels (PCCVs) and liquid gas storage tanks are constructed as bi-directional prestressed concrete (PSC) structures to ensure outstanding leak-tight storage and shielding performance. However, PSC structures exhibit severe vulnerability to high-temperature fire due to the high-strength concrete used and the application of prestressing (PS) stresses to increase the strength of the structures. The PCCV of a 1400 MW advanced power reactor was selected as the target for study. A scaled-down model of the PCCV outer wall was fabricated and tested to determine its resistance to a standard fire-loading scenario. Furthermore, different PS forces were applied to the specimens to evaluate the effect of concrete confinement on the fire resistance. Test data of temperature distribution, PS force loss and residual strength capacity were obtained. The experimental data were used for calibration of a commercial finite-element simulation program (Midas FEA) for structural fire analysis of real-scale concrete structure and infrastructure. The simulation and test results showed significant similarity and the result trends were accurate.

1. Introduction

In the Republic of Korea, although the containment structures of nuclear power plants (NPPs) are designed based on Korean standards, public concern for fire safety of NPPs has recently increased due to the Chernobyl and Fukushima incidents. Moreover, recent global increases in terrorism and war have heightened public anxiety about the catastrophic failures of NPPs. Much effort has thus been put into preventing and mitigating NPP damage and failure under extreme scenarios such as fires, bombings and collisions. In particular, researchers and engineers have focused on the fire safety of prestressed concrete containment vessels (PCCVs) with bi-directionally prestressed reinforced concrete (PSRC) walls, which are highly vulnerable to instantaneous high-temperature fire. The ultimate goal of the design of PCCVs is to ensure fire prevention in possible intense fire accidents, which could lead to structural collapse, economical losses and human casualties (Chang *et al.*, 2006; Ha *et al.*, 2010; Kang *et al.*, 2016; Shin *et al.*, 2008; Won *et al.*, 2006).

In the 1990s, the South Korean Disaster Prevention Agency, the Society for Disaster Prevention and the National Institute for Disaster Prevention conducted studies on human-induced explosions and fire disasters. They mainly focused on disaster prevention and evacuation logistics rather than the prevention of structural damage (AAFNDSWA, 1997; Baker, 1973; Huo *et al.*, 2009; Hyde, 1992; Kakogiannis *et al.*, 2013). When a fire disaster involves a PCCV, prevention should occur at the structural level in order to avoid radiation emission; this level

of fire damage prevention can be ensured by evaluating the thermal conductivity and heat resistance of the PCCV at the design stage. To this end, PCCV walls must be thoroughly tested under realistic fire loading, such as the Richtlinien für die Ausstattung und den Betrieb von Straßentunneln (RABT) fire-loading curve. The RABT fire curve was developed considering an accidental fire in a petroleum tank truck inside a tunnel with the fire temperature reaching 1200°C within 5 min, maintained for 60 min and followed by gradual cooling to ambient temperature within 120 min. However, since real-scale PCCV fire experiments are impossible to conduct due to the high costs and limited availability of testing sites, fire simulations of real-scale PCCVs using calibrated finite-element (FE) simulation programs such as high-fidelity physics-based (HFPB) software are the only way to evaluate the fire resistance of PCCVs accurately. HFPB programs include precise constitutive models, structural models (i.e. prestressing (PS) tendons, steel reinforcements, component dimensions and boundary conditions) and accurate fire-loading parameters, which must be calibrated with actual fire test data. To be considered an effective performance evaluation tool, the accuracy of the results must be within 95% of the test data.

In this study, RABT fire tests were conducted on bi-directional prestressed concrete (PSC) panels with dimensions of $1400 \times 1000 \times 300$ mm by embedding four thermocouples at various depths along the panel thickness direction. The commercial FE program MIDAS-FEA was then used to

Structures and Buildings
Volume 174 Issue 9

Fire resistance of bi-directionally
prestressed concrete under extreme
fire loading
Choi, Yang, Choi, Yi and Kim

simulate the fire test to calibrate the program to determine whether MIDAS-FEA can be employed as an HFPB simulation program. After the calibration, a parametric study was performed on the PSC panels, considering variables such as concrete strength, cover thickness, PS force and reinforcement ratio. The simulations results were used to evaluate the fire resistance, thermal failure mode, energy absorption capacity, PS force loss, heat transfer distribution, surface damage area and spalling depth of the PSC walls.

2. Literature review

2.1 Concrete thermal spalling

Menzel (1943) and Gustaferro and Selvaggio (1967) investigated the thermal characteristics of concrete at high temperature. These characteristics can be mainly divided into physical (e.g. unit volume weight, weight loss rate, specific heat, thermal conductivity and thermal expansion rate) and mechanical properties (e.g. compressive strength, elastic modulus, stress–strain curve and creep). A study on the physical characteristics of normal-strength concrete (NSC) and lightweight concrete heated to high temperatures revealed that the specific heat is closely dependent on the type of aggregate used in the mix. The aggregate type also has a strong effect on thermal conductivity and the heat expansion ratio (Schmeider, 1986).

Research on the thermal characteristics of high-strength concrete (HSC) began in the 1990s. Studies on specimen size, fire temperature and concrete strength indicated that the concrete density directly influences the degree of thermal spalling (Hammer, 1995; Hertz, 1991). Hammer (1995) analysed the loss of strength of HSC and reported that it was due to the spalling caused by a large amount of free-water vaporisation at 300°C. Simultaneously, a reduction in Young's modulus occurred at similar or higher temperatures. Concrete thermal spalling is the most serious damage that can occur during a fire. It involves partial loss of concrete volume and surface area due to catastrophic cracking and exfoliation. Thermal spalling generally originates from interactions among various factors, such as fire temperature, thermal stress distribution, aggregate mineral composition and water content. The expansion of internal voids due to free water transforming into vapour also induces thermal spalling. Given its low thermal conductivity and high specific heat, concrete is a good fire-resistant material. However, its low thermal conductivity generates two- or three-dimensional thermal tensile stresses within the matrix. When the tensile stress in the matrix exceeds the tensile strength of the concrete, cracking or exfoliation occurs (Anderberg, 1997). Similar behaviour is observed in curved-surface concrete members and flat-surface concrete members (Kalifa et al., 2000).

The behaviour of moisture in concrete is as follows. The concrete surface desorbs water when heated by fire loading; most of the as-formed water vapour is transported to the concrete inside, which is cooler, and is re-absorbed by pores. If heat is applied continuously, both water and water vapour accumulate in the internal voids as the surface temperature gradually increases. The rate of water vapour transport varies with the heating rate and the internal pore structure. Water vapour cannot move quickly through the pores due to the presence of a saturated layer below the heated surface, which possibly causes water evaporation at the contact surface. Moreover, a rapid temperature increase, restrained expansion and rapid enhancement in the water vapour pressure occur. If the concrete tensile strength cannot restrain the tensile stress generated by the water vapour pressure, thermal spalling with fragmentation and exfoliation occurs at the concrete surface. A schematic diagram of the thermal spalling mechanism is shown in Figure 1 (Choi, 2013). Thermal spalling generally occurs within 20–30 min after the start of fire loading for both NSC and HSC. However, the failure mode of thermal spalling is much more catastrophic in HSC than in NSC because the pore pressure release in the former cannot escape while gradual pore pressure release is possible in the latter due to its relatively lower density.

2.2 Fire curves

Cellulosic fire curve regulations are specified in many standards (e.g. KS F 2257 (KSA, 1999), ISO 834 (ISO, 1980), BS 476: Part 20 (BSI, 1987), DIN 4102 (DIN, 1998) and AS 1530 (SA, 2005)). A cellulosic curve defines the relationship between the fire duration and temperature change based on the temperature measured through multiple standardised fire tests, which are designed to evaluate the fire resistance of general building materials. Figure 2 shows these curves for the fire scenarios specified in the Korean standard KS F 2257, which is used to test building members such as walls, columns, beams and ceilings. However, the fire-resistance regulations associated with these general building structures are very different from the fire-resistance concept associated with infrastructure such as tunnels and bridges (e.g. fire resistance measured under rapidly rising temperature).

1. Evaporation of pore water

2. Transport of material mass

3. Steam barrier due to saturated zone

4. Spalling due to steam pressure
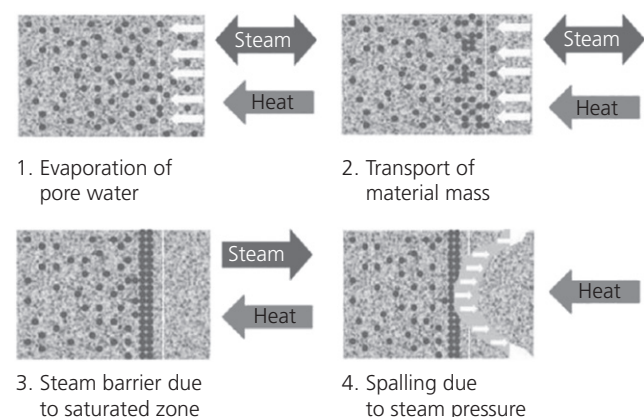
Figure 1. Thermal spalling mechanism

Structures and Buildings
Volume 174 Issue 9

Fire resistance of bi-directionally
prestressed concrete under extreme
fire loading
Choi, Yang, Choi, Yi and Kim
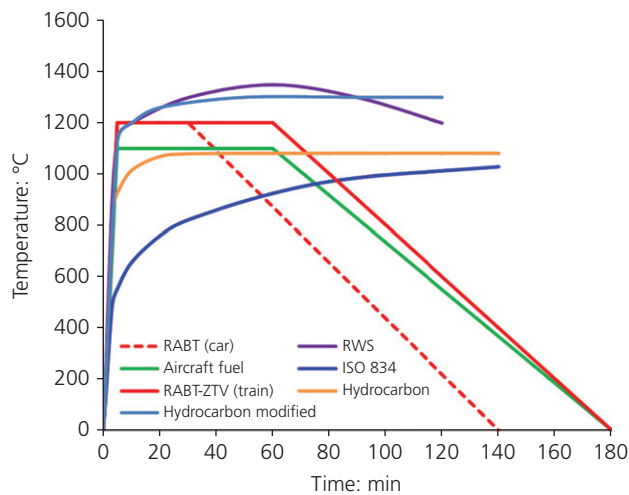
Figure 2. Various fire curves

The time–temperature histories of combustion due to the ignition of chemicals or petrochemical products have different trends compared with cellulosic fire curves. For this reason, a hydrocarbon fire curve was developed (Figure 2). Hydrocarbon curves – which induce extremely high temperatures within short time duration – are used to represent the fire behaviours of oil tank trucks, ships and factories and buildings where chemical materials are manufactured. In a hydrocarbon curve, the temperature rapidly increases above 850°C, gradually reaches 1080°C within 30 min and then remains constant.

In 1979, the Rijkswaterateaat (RWS) curve was developed following fire tests conducted in the Rijkswaterateaat tunnel by TNO in the Netherlands (Figure 2). The RWS curve was developed for the most severe scenario of a heat emission rate of 300 MW fire loading, similar to a fire ignited from an oil tanker truck filled with petroleum burning inside a tunnel for more than 120 min (as compared with 60 min in the RABT curve). More specifically, in the RWS curve, the temperature increases above 1400°C within 5 min, gradually reaches the maximum value and finally decreases slowly to ambient temperature. A full-scale test was recently performed in the Runehamar tunnel in Sweden using the RWS curve.

In 1990–1992, the RABT curve was developed in Germany as an output from the Eureka 499 project. In the RABT curve, the temperature reaches 1200°C within 5 min, is maintained for 30 min and then reduces to ambient temperature within 100 min (Figure 2). The RABT curve is based on full-scale fire tests with vehicles, large trailers, fuel-driven trains and electricity-driven trains with a maximum temperature maintenance time of at least 30 min, 60 min, 80 min and 5 min, respectively. Furthermore, the cooling time can also vary depending on the fire type and the surrounding conditions.

In the study reported in this paper, the following fire scenario was assumed: an airplane collision or bomb explosion on the outer wall surface of a PCCV leading to instantaneous ignition with the maximum temperature from the jet fuel exceeding 1100°C in the initial stage. The fire test was conducted using the RABT fire curve (as specified by the Korean Ministry of Transportation and Road Construction) because this curve best fits the assumed scenario.

3. Experimental details

3.1 Specimen details

To evaluate the fire resistance of concrete panels, three types of specimens were prepared: reinforced concrete (RC), prestressed concrete without rebars (PSC) and prestressed concrete with rebars (PSRC). Three types of specimens were considered in order to obtain test data for three types of failure behaviour under the RABT fire loading to calibrate FE simulation models to be used in the future for real-scale concrete structure simulations. As expected, the three different specimen types showed dramatically different thermal failure behaviours due to different structural mechanisms owing to the presence of rebars and PS tendons. The design criterion of the specimens followed the actual outer wall design of a PCCV other than a smaller wall thickness. The only design parameter variation in the specimens was the PS force variation from using steel wire and strands for prestressed concrete (SWPC) 7B and 7D strands.

The specimen dimensions were $1400 \times 1000 \times 300$ mm (Figure 3). D13 rebars with a mesh configuration of 100 mm spacing were placed at the top and bottom of the RC and PSRC specimens. All the specimens were cast with concrete with a 28-day concrete compressive strength of 40 MPa. The mix design of the concrete, which is the same as the concrete used to cast actual PCCVs, is shown in Table 1.

The specimens were moved to the fire test site 28 days after concrete pouring. The fire tests were conducted 15–17 days after the arrival at the test site. Therefore, the age of the concrete at time of testing was 43–45 days from the initial casting date. Unfortunately, the moisture content of the concrete was not checked prior to the test and therefore no moisture content data are available. The PS force was applied using a 15.2 mm PS strand. To study the effect of the PS force on the fire behaviour of a biaxial PSC panel, two types of steel strands were used: SWPC 7B (B-type), with a yield strength of 1600 MPa, ultimate strength of 1730 MPa and unit weight of 1.101 kg/m, and SWPC 7D (D-type), with a yield strength of 2040 MPa, ultimate strength of 2400 MPa and unit weight of 1.101 kg/m. The rebar and tendon ratios were 0.024 and 0.0107, respectively, for the PCCV outer wall. The steel liner plate typically placed on the inner surface of a PCCV wall to prevent radiation leakage was excluded in this study in order to assess the concrete structural failure

Structures and Buildings
Volume 174 Issue 9

**Fire resistance of bi-directionally
prestressed concrete under extreme
fire loading**
Choi, Yang, Choi, Yi and Kim
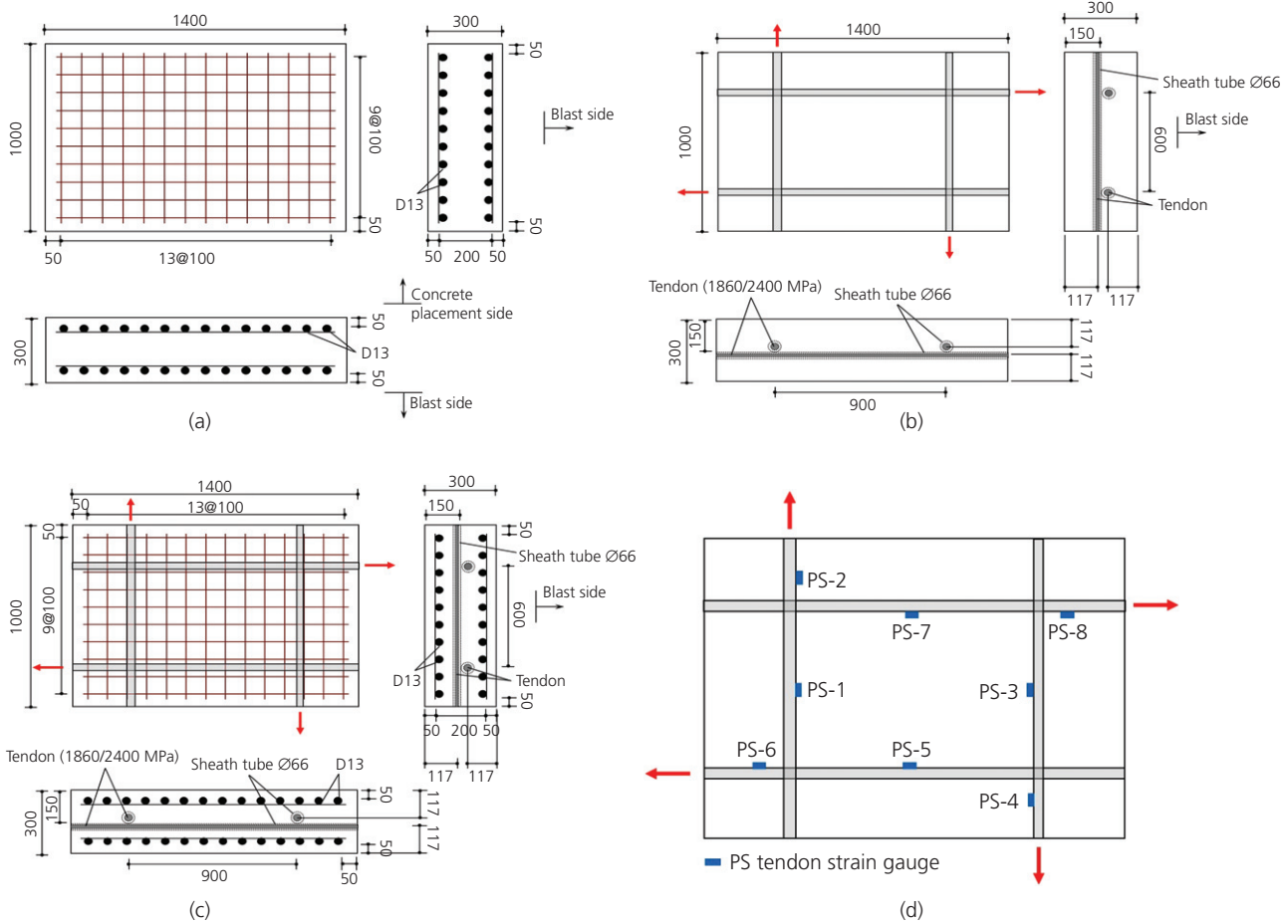
Figure 3. Specimen types and details: (a) RC; (b) PSC; (c) PSRC; (d) PS tendon gauge locations (dimensions in mm)

Table 1. Concrete mix proportions

				Unit weight: kg/m³					
					Binder				
MCA: mm	Slump: mm	W/B: %	S/A: %	W	C	GGBS	S	G	AE
25	180	33	45.5	165	425	75	786	918	4.0

MCA, maximum size of coarse aggregate; W/B, water/binder ratio; S/A, fine to total aggregate ratio; W, water; C, cement; GGBS, ground granulated blast-furnace slag; S, unit weight of fine aggregate; G, unit weight of coarse aggregate; AE, air-entraining agent

behaviour under fire loading conservatively. An 80 mm unbonded-type sheath tube was fabricated and installed, as shown in Figure 3(b). The PS force was measured by attaching strain gauges at various locations in the specimens during their fabrication. Strain gauges PS-1, PS-3 and PS-5, PS-7 were attached on the midspan of the PS tendons in the shorter and longer width direction, respectively; gauges PS-2, PS-4 and PS-6, PS-8 were attached 200 mm from the PS anchorage on the tendons in the shorter and longer width directions, respectively. The actual PS force applied to the B-type and D-type tendons

was 520–610 kN and 690–820 kN, respectively. All the PS tendon strain gauge locations are shown in Figure 3(d).

3.2 Fire test setup
The fire test was performed at the Korea Institute of Construction Technology using a gas heating furnace to apply the RABT fire loading (Figure 4). To test a scenario of applying an external fire load exceeding 1200°C (such as aircraft fuel burning on the surface of a PSC nuclear containment vessel), a test setup of a fire burner separated from the

Structures and Buildings
Volume 174 Issue 9

Fire resistance of bi-directionally
prestressed concrete under extreme
fire loading
Choi, Yang, Choi, Yi and Kim

Figure 4. Heating system

4. Experimental results and discussions

4.1 Surface examination and crack patterns
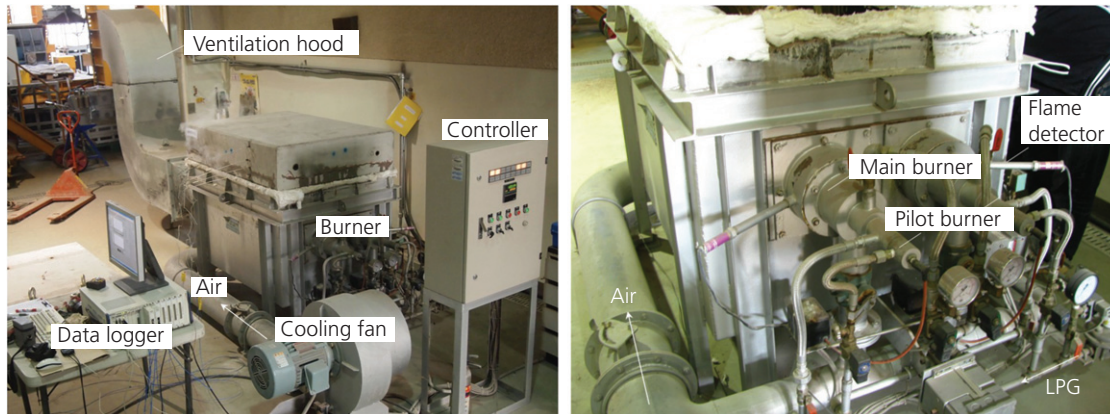
loading actuator is required. Unfortunately, there is no test site with such an apparatus available in Korea to conduct this type of extreme fire test. Therefore, the decision was made to select the limited scope of a fire test condition of not applying an external load while fire was applied up to 1200°C to evaluate the PSC specimen behaviour under fire.

The temperature was increased to 1200°C within 5 min and maintained for 60 min, followed by gradual cooling to ambient temperature in 120 min. The furnace applied fire to the bottom surface of the panel, which was installed at the top opening of the furnace. The test method strictly followed the Korean fire test standard (KS F 2257-1). Concrete exfoliation due to thermal spalling occurred on both the fire-applied surface and the side surfaces. K-type thermocouples were placed at quarter-width locations bisecting the centre line and the edge of the panels at different depths (50, 100, 150 and 250 mm) from the fire-applied surface (Figure 5). Temperature data were collected using a DS-NET data logger.

Figures 6–11 illustrate the surface damage and crack patterns of the specimens under the RABT fire loading. Further details are provided in Table 2. As shown in Figure 6, the PSC and PSRC specimens showed much greater thermal spalling than the RC specimen. The bottom rebars if the RC specimens were exposed due to thermal spalling (Figure 7(a)), meaning they were in direct contact with the fire. The maximum exfoliation depth was 48 mm (Table 2). Nonetheless, the PSC and PSRC specimens experienced more significant thermal spalling than the RC specimen (Figures 8(a)–11(a)). The damage exfoliation depths of the PSC(B) and PSC(D) specimens were 199 mm and 192 mm, respectively. Moreover, the tendons were exposed due to burning of the pre-installed sheath tube. The exfoliation depths of PSRC(B) and PSRC(D) were 167 mm and 161 mm, respectively, indicating that the top rebars were partially exposed while the bottom was fully
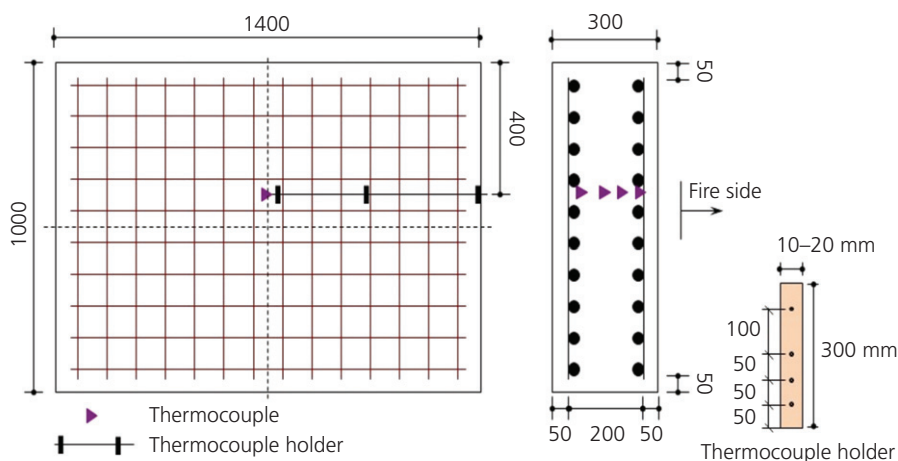
Figure 5. Thermocouple locations (dimensions in mm)

Structures and Buildings
Volume 174 Issue 9

Fire resistance of bi-directionally
prestressed concrete under extreme
fire loading
Choi, Yang, Choi, Yi and Kim
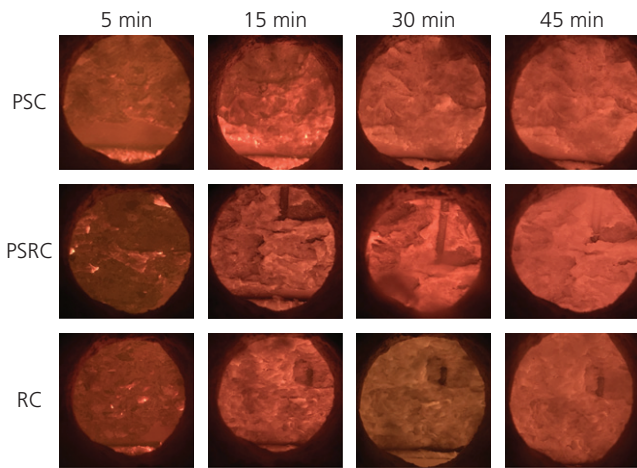
Figure 6. Damaged surfaces of fire test specimens

exposed. However, no fire damage was observed in the sheath tubes. After fire loading, the top sides of the PSC and PSRC specimens showed smaller cracks than the RC specimen. Both the PSC and PSRC specimens showed cracks in the midspan and the majority were located along the shorter width direction.

The areas damaged by fire loading were 7.46×10^6, 8.82×10^6, 8.59×10^6, 7.50×10^6 and 7.59×10^6 m^2 for the RC, PSC(B),

PSC(D), PSRC(B) and PSRC(D) specimens, respectively. However, the corresponding damage volumes calculated considering the maximum exfoliation depth were 35.79×10^6, 175.58×10^6, 164.94×10^6, 63.53×10^6 and 55.80×10^6 mm^3, respectively. In other words, the damage volumes of the PSC (B), PSC(D), PSRC(B) and PSRC(D) specimens were, respectively, 4.91, 4.61, 1.77 and 1.56 times larger than that of the RC specimen. The RC specimen showed the least fire damage and had no PS confinement. The PSC and PSRC specimens with PS confinement showed significant damage due to thermal spalling and exfoliation. Moreover, the occurrence of thermal spalling varied with the PS force magnitude, resulting in different damage degrees. The PSC(D) and PSRC(D) specimens (with a PS force of 820 kN) showed 2.54% and 1.84% less damage than the PSC(B) and PSRC(B) specimens (PS force of 580 kN(, respectively. Both the PSC and PSRC specimens subjected to PS confinement exhibited exfoliation damage from severe thermal spalling. However, the results of fire damage rate revealed that the specimens with stronger confinement stresses showed better resistance to fire loading with less thermal damage.

4.2 Time–temperature relationships
The time–temperature histories obtained from the K-type thermocouples are shown in Figure 12; the temperature data are summarised in Table 3. Under the RABT fire loading, the RC specimen exhibited an exfoliation depth up to 50 mm,
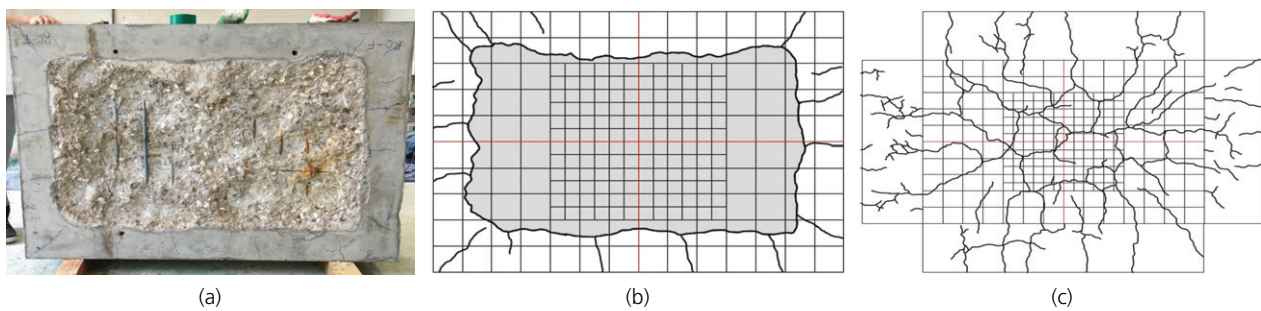
Figure 7. Damaged surface and crack patterns of RC specimen: (a) damaged surface; (b) top surface; (c) bottom surface
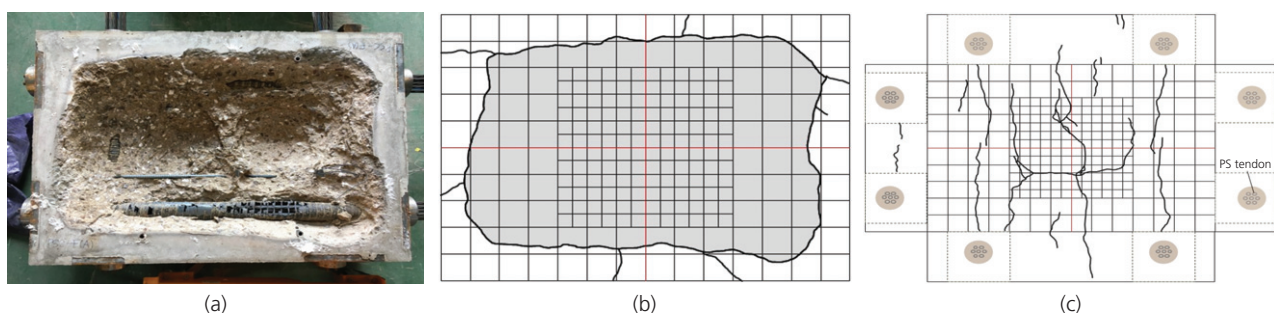
Figure 8. Damaged surface and crack patterns of PSC(B) specimen: (a) damaged surface; (b) top surface; (c) bottom surface

Structures and Buildings
Volume 174 Issue 9

**Fire resistance of bi-directionally
prestressed concrete under extreme
fire loading**
Choi, Yang, Choi, Yi and Kim
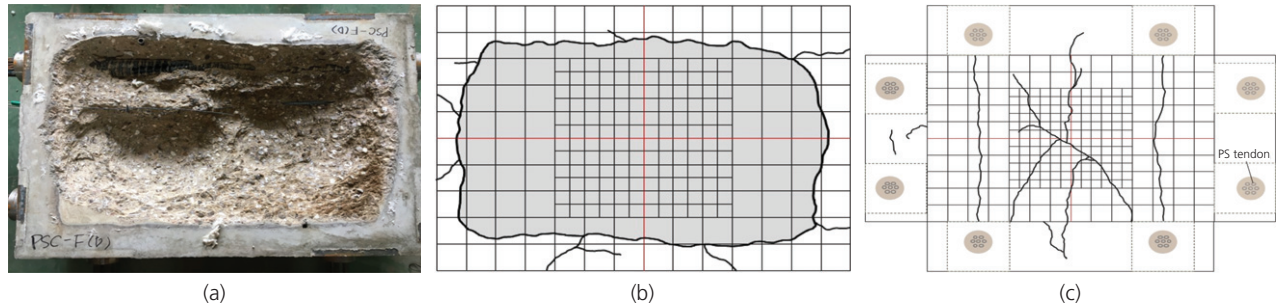
Figure 9. Damaged surface and crack patterns of PSC(D) specimen: (a) damaged surface; (b) top surface; (c) bottom surface
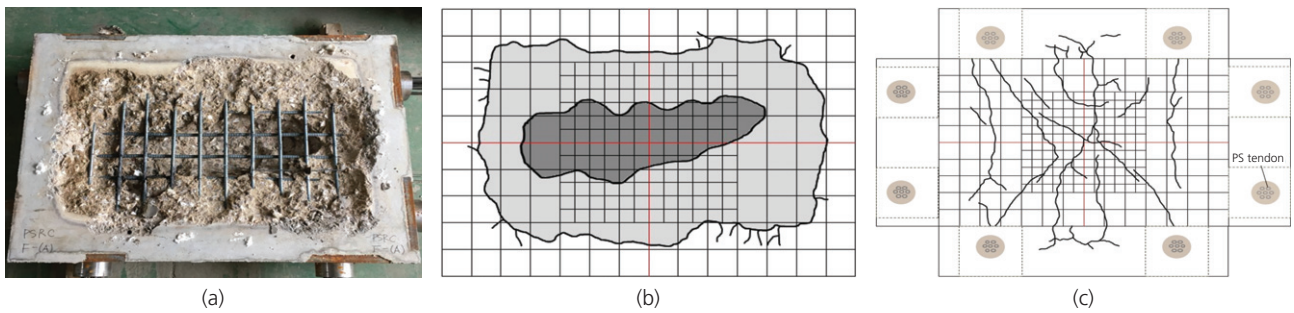
Figure 10. Damaged surface and crack patterns of PSRC(B) specimen: (a) damaged surface; (b) top surface; (c) bottom surface
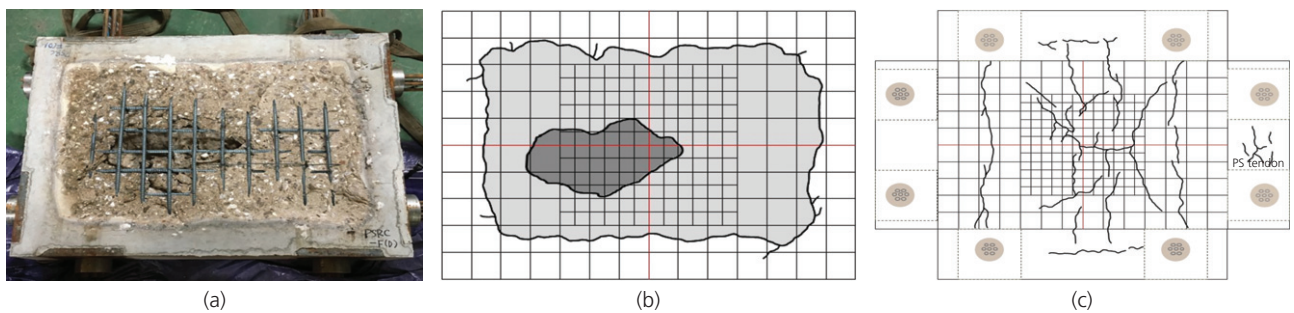
Figure 11. Damaged surface and crack patterns of PSRC(D) specimen: (a) damaged surface; (b) top surface; (c) Bottom surface

Table 2. Approximate maximum damage calculations from the test data

Specimen	Maximum damage depth: mm	Surface damage area: 10^5 mm^2		Damage volume: 10^6 mm^3	Damage rate: %
RC	48	7.46		35.79	8.52
PSC(B)	199	8.82		175.58	41.81
PSC(D)	192	8.59		164.94	39.27
PSRC(B)	167	Centre	1.68	35.48	6.67
		Exterior	5.82	28.03	8.45
		Total	7.50	63.53	15.12
PSRC(D)	161	Centre	0.94	15.21	3.62
		Exterior	6.65	40.59	9.66
		Total	7.59	55.80	13.28
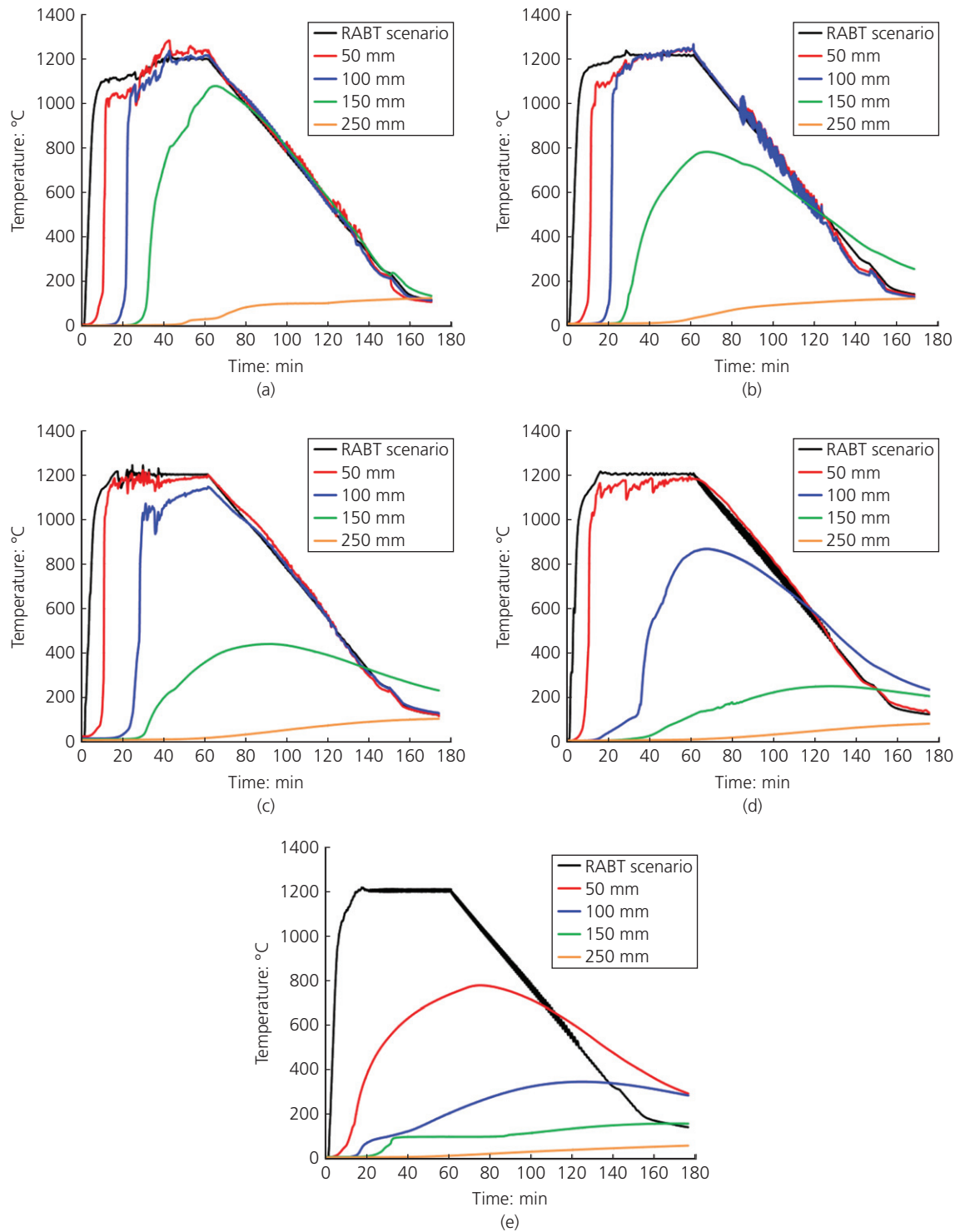
Figure 12. Temperature–time history curves of fire-damaged specimens: (a) PSC(B); (b) PSC(D); (c) PSRC(B); (d) PSRC(D); (e) RC

which was the cover depth of the bottom rebar from the heated surface. The exfoliation depths of the PSC and PSRC specimens were 150–250 mm. The thermocouples placed at 150 mm depth of the PSC specimen with 200 mm exfoliation

depth from the heated surface provided a temperature measurement of 1080°C (Figure 12(a)). At a depth of 50 mm (equivalent to the concrete cover thickness) from the heated surface, all the specimens except the RC specimen (Figure 12(e)) showed

Table 3. Maximum temperatures of specimens at different depths as a result of fire loading

Specimen	Maximum measured temperature: °C			
	50 mm	100 mm	150 mm	250 mm
RC	777.86	345.72	157.67	58.39
PSC(B)	1285.72	1241.79	1080.50	127.52
PSC(D)	1249.96	1256.36	774.65	120.14
PSRC(B)	1224.03	1148.67	440.28	102.27
PSRC(D)	1191.86	868.04	248.90	79.12

the same temperature behaviour as the RABT fire curve due to rebar exposure in the specimens as a result of thermal spalling induced exfoliation. The rebar exposure in the PSC specimens led to thermal stress yielding after only 20 min from the start of the RABT fire loading. After the occurrence of thermal spalling damage in the PSC and PSRC specimens, the PS force in the tendons decreased continuously until the end of the test.

The temperature histories of the PSC specimens confirmed significant thermal spalling during the fire loading. The

Table 4. Fire damage criteria for nuclear containment vessels and tunnels

Nuclear containment vessels				Tunnels		
Design temperature: °C				Maximum operation temperature: °C		
KSNP[a]	APR 1400[b]	ASME (2010)		JCI (2002)	ITA (2004)	RWS
141	143	175/345	Concrete	250–380	380	380
			Steel	250–380	250	500

[a]Korea Standard Nuclear Power Plant
[b]1400 MW advanced power reactor
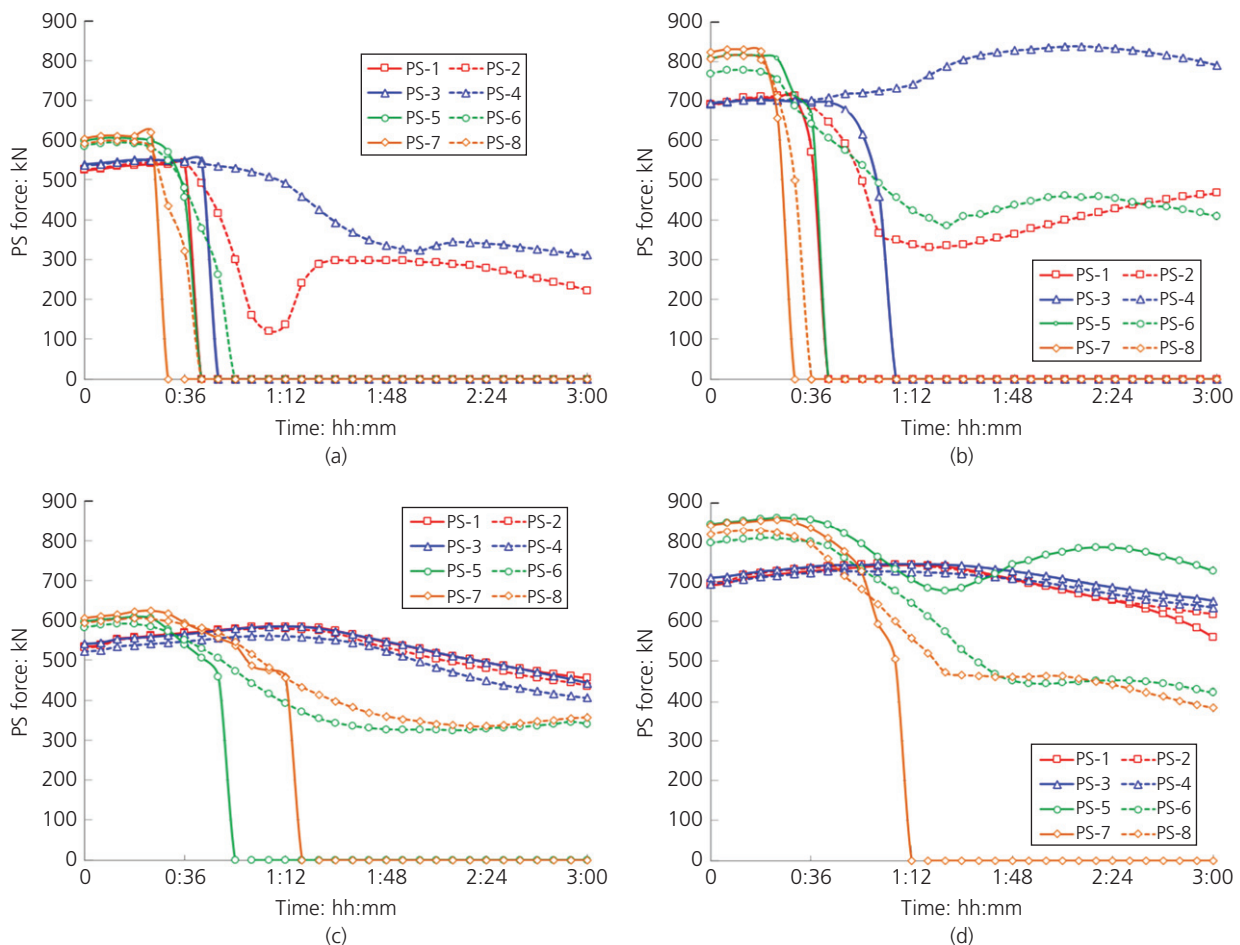
Figure 13. PS force history curves under fire loading: (a) PSC(B); (b) PSC(D); (c) PSRC(B); (d) PSRC(D)

Structures and Buildings
Volume 174 Issue 9

**Fire resistance of bi-directionally
prestressed concrete under extreme
fire loading**
Choi, Yang, Choi, Yi and Kim

temperature distributions of the PSC and PSRC specimens according to the difference in the PS force revealed that the maximum temperature of PSC(B) at a depth of 150 mm was 305.85°C higher than that of PSC(D), and the temperature of PSRC(B) at 100 mm was 280.63°C higher than that of PSRC(D). These results indicate that thermal spalling occurred

(a)   (b)

Figure 14. Fire damage of (a) PS tendon and (b) sheath tube

Table 5. PS force losses of PSC specimens

	PSC(B)				PSC(D)			
	Load: kN				Load: kN			
	Before heating	After heating	Loss: kN	Loss rate: %	Before heating	After heating	Loss: kN	Loss rate: %
Shorter width direction								
PS-1	524.95	N[a]	N	N	692.22	N	N	N
PS-2	526.12	223.86	−302.26	57.45	691.56	434.54	−256.98	37.16
PS-3	538.60	N	N	N	693.72	N	N	N
PS-4	535.94	306.12	−229.52	42.83	696.22	579.21	−117.01	16.81
Longer width direction								
PS-5	597.52	N	N	N	808.07	N	N	N
PS-6	584.54	N	N	N	769.78	393.29	−376.49	48.91
PS-7	603.18	N	N	N	823.38	N	N	N
PS-8	591.03	N	N	N	806.24	N	N	N

[a]Not available

Table 6. PS force losses of PSRC specimens

	PSC(B)				PSC(D)			
	Load: kN				Load: kN			
	Before heating	After heating	Loss: kN	Loss rate: %	Before heating	After heating	Loss: kN	Loss rate: %
Shorter width direction								
PS-1	533.94	455.38	−78.56	14.71	690.23	577.22	−113.01	16.37
PS-2	531.61	456.71	−74.90	14.09	696.05	618.16	−77.89	11.19
PS-3	540.60	446.72	−93.87	17.36	708.70	654.28	−54.42	7.68
PS-4	521.79	403.45	−118.34	22.68	693.89	635.47	−58.42	8.42
Longer width direction								
PS-5	596.19	N[a]	N	N	844.35	732.34	−112.01	13.27
PS-6	582.54	329.05	−253.49	43.51	796.42	405.29	−391.13	49.11
PS-7	605.51	N	N	N	843.02	N	N	N
PS-8	593.03	338.37	−254.65	42.94	819.38	362.67	−456.71	55.74

[a]Not available

Structures and Buildings
Volume 174 Issue 9

**Fire resistance of bi-directionally
prestressed concrete under extreme
fire loading**
Choi, Yang, Choi, Yi and Kim
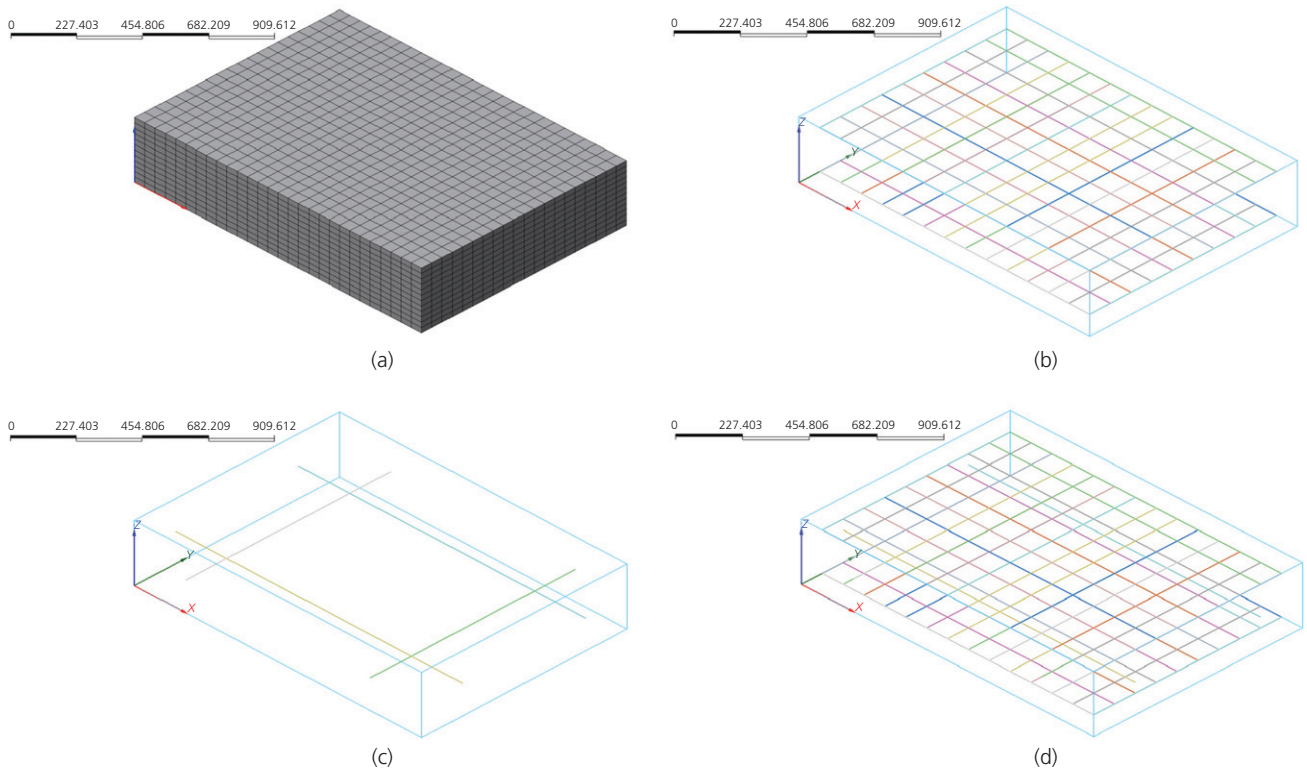
Figure 15. Specimen modelling details: (a) concrete; (b) RC; (c) PSC; (d) PSRC

similarly during the early heating stage due to the applied confinement stresses; however, spalling was reduced when these stresses increased due to the higher PS force, which indicates that PSC members with higher confinement stress have better fire resistance.

The International Tunneling Association (ITA) reported that explosive spalling occurs largely at the beginning of a fire and stops once the fire has progressed to some extent (ITA, 2004). In the present study, the RC specimen suffered explosive spalling up to the depth of the rebar cover thickness from the heated surface at the early stage of fire, which is consistent with the ITA report, followed by rebar degradation beyond 15 min exposure. However, for the PSC and PSRC specimens, explosive spalling began at the early stage of fire loading and continued even after 30 min of heating. The specimens were damaged by fire all through the test due to crack closing owing to the application of the PS force. This indicates that explosive spalling of PSC members can vary due to variations in the confinement stresses, which is in contrast to the ITA findings. Furthermore, a comparison of the service limit temperatures for tunnel structures and design temperatures for nuclear containment structures (Table 4) suggests that both the RC and PSC specimens should be considered dangerous without the use of fire-proof materials based on the service limit temperatures proposed by various nations. The design temperature proposed for PCCV accidents is 3.12–8.68 times

higher for PSC and PSRC elements than for RC ones. The ITA suggests using the ISO 834 fire curve for PCCV design (ITA, 2004); however, further investigations on the service and design temperatures of fire-proof materials are required to better prepare for fire incidents.

4.3 PS force loss
Cold-rolled steel used to fabricate PS strands for unbounded prestressed members is more sensitive to temperature increase than mild steel. Therefore, the PS force loss due to fire
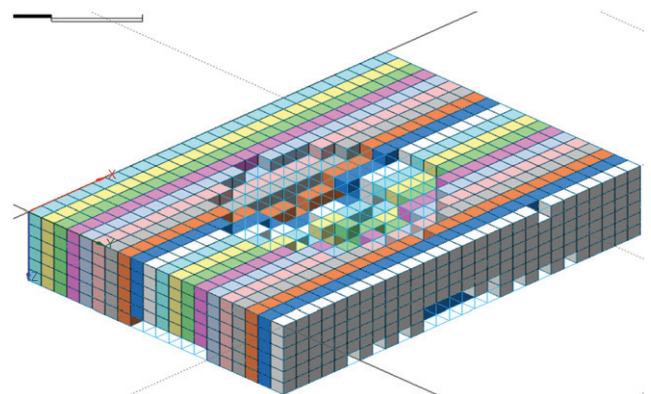
Figure 16. Thermal spalling model for fire simulation

Structures and Buildings
Volume 174 Issue 9

Fire resistance of bi-directionally
prestressed concrete under extreme
fire loading
Choi, Yang, Choi, Yi and Kim

loading needs investigation. The PS force of the tendons was studied by applying the selected RABT fire loading. The variations in the PS forces obtained from the tests are

shown in Figure 13. Under the RABT fire loading, the PSC specimens experienced thermal spalling due to the strong confinement stresses over 60 min when the PS force increased.
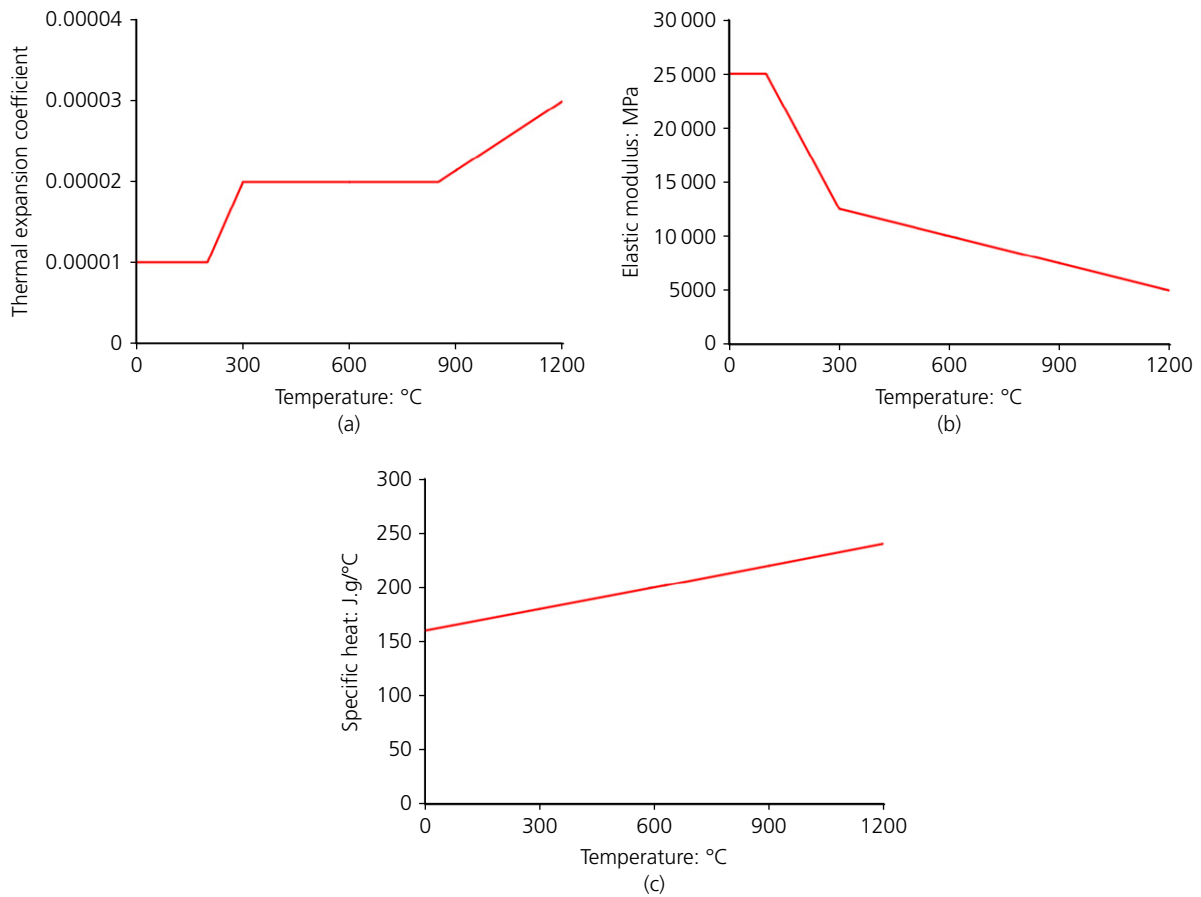
Figure 17. Concrete thermal constitutive models: (a) thermal expansion coefficient; (b) elastic modulus; (c) specific heat
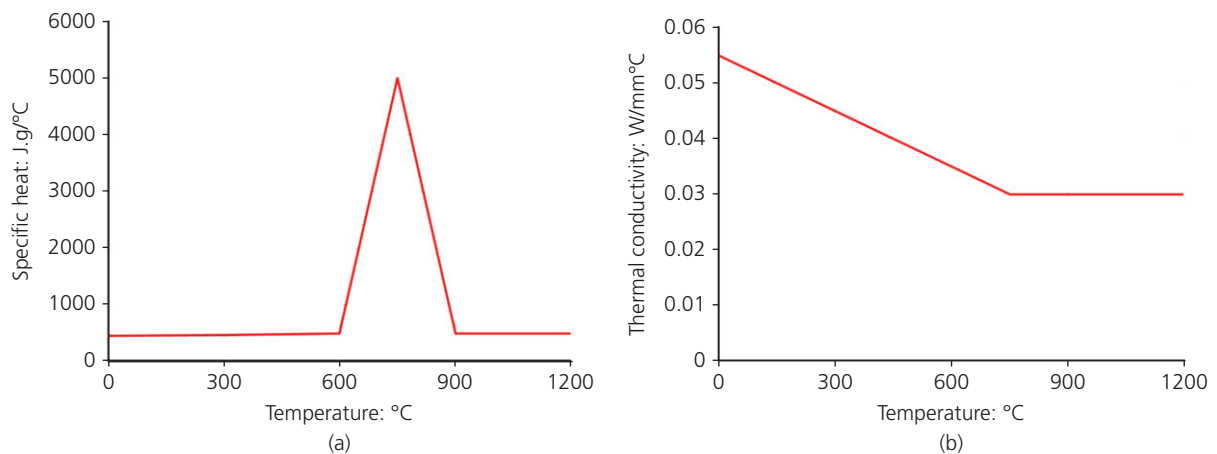
Figure 18. Steel thermal constitutive models: (a) specific heat; (b) thermal conductivity

Structures and Buildings
Volume 174 Issue 9

**Fire resistance of bi-directionally
prestressed concrete under extreme
fire loading**
Choi, Yang, Choi, Yi and Kim

Owing to this, the sheath tube of the tendons burned away
(Figure 14) and most of the strain gauges attached to the
tendons were destroyed. In contrast, the PSRC specimens
experienced less thermal spalling than the PSC specimens and
therefore their PS force variations could be measured through-
out the 180 min of testing. When a fire loading of 1200°C was
maintained, the PS forces increased slightly due to thermal
expansion of the tendons. From the cooling down stage until
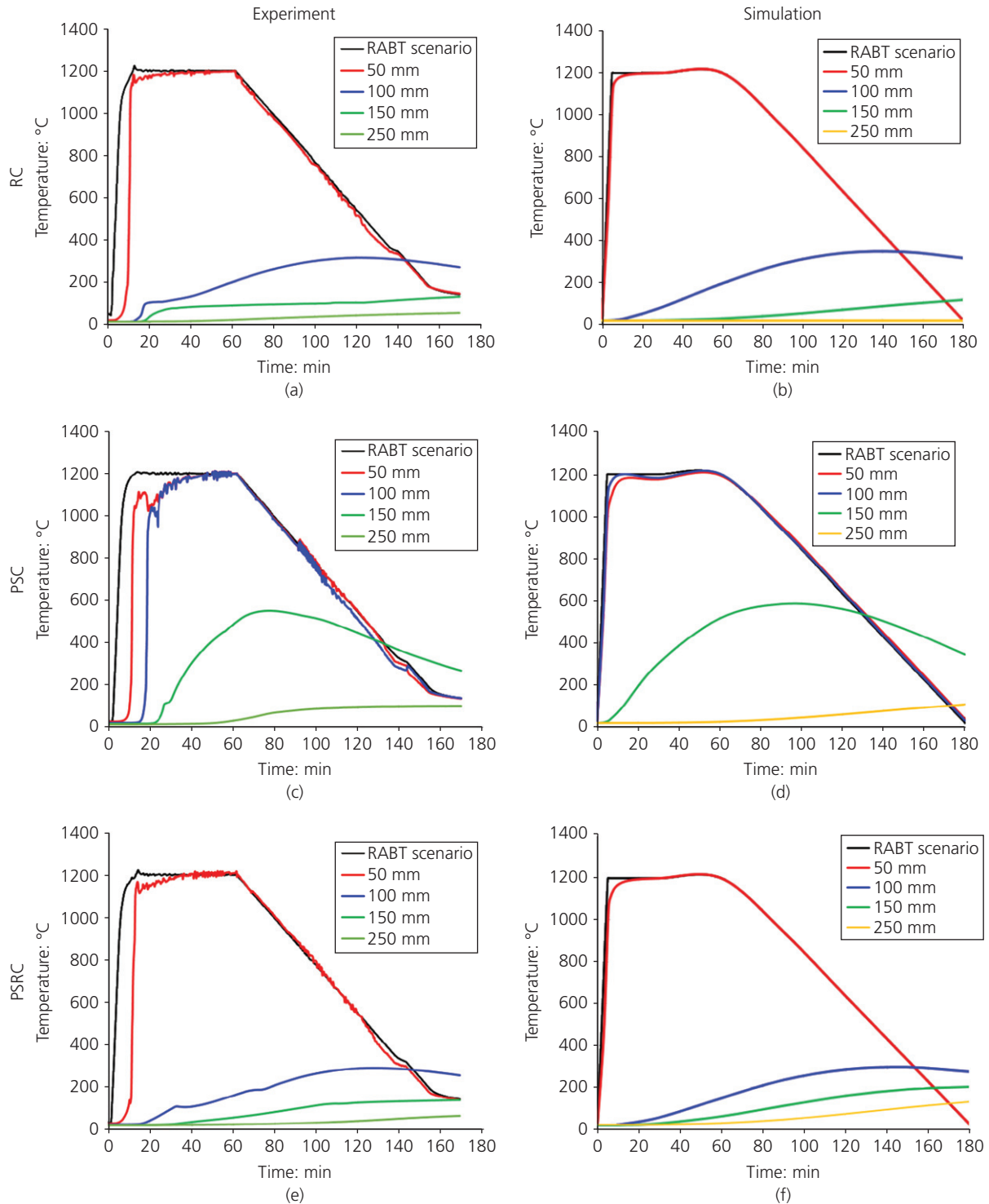
Figure 19. Temperature–time history curves: test and simulation results

ambient temperature was reached, the PS forces decreased rapidly.

As shown in Table 5, for the PSC(B) specimen, the PS force loss rates in PS-2 and PS-4 (on the tendons located near the side of the panel along the shorter width direction) were 57.45% and 42.83%, respectively. However, gauges PS-1 and PS-3 (attached to the tendons located in the middle region along the shorter width direction) and PS-5–PS-8 (the tendons along the longer width direction) were all damaged by the fire and thus could not acquire data. For PSC(D), the PS force loss rates in PS-2 and PS-4 (the tendons along the shorter width direction) and in PS-6 (the tendon near the side along the longer width direction) were 37.16%, 16.81% and 48.91%, respectively. The PS loss rates of PSRC(B) were 14.09–22.68% along the shorter width direction and 42.94–43.51% along the longer width direction, while the corresponding losses for PSRC(D) were 7.68–16.37% and 49.11–55.74%, respectively (Table 6). These results indicate that the PS force loss in the longer tendon length was much more severe than that in the shorter tendon, which is logical.

5. Verification using numerical simulation

Numerical simulations of the temperature distributions were performed to evaluate the fire resistance performance of the investigated specimens precisely. FE modelling and analysis procedures may vary according to the assessment methodology. In this study, the properties of the rebars and tendons at high temperatures were taken into consideration during the thermal behaviour of the PSC members at high temperatures. The RC, PSC and PSRC specimens were simulated using Midas FEA. The specimen details used in the analysis are shown in Figure 15.

For the concrete constitutive model, the total strain crack model given in the Midas FEA code was used. The necessary parameters were derived from the compressive strength, which was 40 MPa according to 28-day compressive strength testing. The rebars and PS tendons used in the test were modelled as discrete beams embedded in a three-dimensional solid concrete element. The layout and dimensions of the rebars and PS tendons precisely followed those of the experiments. The PS force was applied as the initial condition using the Initial stress beam option in Midas FEA. The initial force applied to the PS tendons was assumed to be maintained throughout the simulation without any loss. The rebar material model considered the isotropic and kinematic hardening plasticity used in the von Mises plasticity model. The steel frame of the gas burner and the specimen were assumed to be perfectly fixed; therefore, the steel frame could be excluded. Thus, the top and bottom edge nodes had fixed boundary conditions.

To evaluate the damage and failure behaviour of the concrete members under extreme fire loading, thermal analyses were conducted using Midas FEA. Thermal spalling induced

by the fire loading was not physically implemented in the simulation. Instead, the spalling effect was considered indirectly by applying temperature-dependent concrete constitutive models.

A physical spalling characteristic was implemented by eliminating all the concrete elements when the maximum concrete thermal tensile strain of 0.0003 was exceeded (Han *et al.*, 2015). Details regarding the concrete elements that needed to be eliminated were obtained from the output data file. Through this process of element elimination, concrete thermal spalling or exfoliation in the PSC specimens could be achieved to show a more realistic fire simulation of the damaged PSC specimen. In other words, if the concrete surface section spalled off and the rebar was exposed, the specimens with an exfoliated concrete surface would undergo greater thermal damage than those without spalling damage. Figure 16 shows the concrete simulation model with concrete thermal spalling. The feasibility of this approach was verified by Choi *et al.* (2017).

5.1 Heat transfer constitutive models

The material properties and structural behaviour of structures and infrastructure change significantly over time in the event of thermal loading. Heat transfer analysis was thus conducted with the aim of evaluating the temperature distributions in fire-loaded structures according to the material heat transfer properties and the structural responses (strain and stress) caused by high-temperature loading. The constitutive models shown in Figure 17 were employed to determine the thermal characteristics of the concrete (i.e. the thermal expansion coefficient, elastic modulus and specific heat) to analyse high-temperature heat transfer. The constitutive models shown in Figure 18 were used to determine the thermal characteristics of the rebars and PS tendons (i.e. specific heat and heat conductivity). Although BS EN 1992-1-1:2004 (BSI, 2004) presents a concrete thermal conductivity within the range 1.36–2.3 W/m°C based on the concrete temperature, previous studies have reported significant differences between

Table 7. Comparison of experimental and analytical temperatures at different depths

	Temperature: °C			
	50 mm	100 mm	150 mm	250 mm
RC				
Experiment	777.87	345.72	157.67	58.39
Analysis	748.51	335.11	158.74	29.20
PSC				
Experiment	1285.72	1241.79	1080.50	127.52
Analysis	1195.60	1193.37	1045.86	145.99
PSRC				
Experiment	1224.03	1148.67	440.28	102.27
Analysis	1195.63	1125.33	440.40	88.86

Structures and Buildings
Volume 174 Issue 9

Fire resistance of bi-directionally
prestressed concrete under extreme
fire loading
Choi, Yang, Choi, Yi and Kim

simulation and experimental results when using this thermal conductivity range (Choi *et al.*, 2017). However, when a general range for the thermal conductivity of concrete was used in the fire simulation, the simulation results were very different to the experimentally measured temperature data. The thermal conductivity of concrete shows large variations depending on the aggregate type, specific gravity and concrete strength. In addition, it is very sensitive to surrounding temperatures such as burning or freezing conditions. Therefore, the thermal conductivity must be determined experimentally. In this study, to calibrate the fire simulation model to accurately represent the fire test conditions, a thermal conductivity range approximately five times that proposed in BS EN 1992-1-1:2004 (i.e. 5.9–12.0 W/m °C) was used in the fire simulation.

5.2   Comparison of simulations and fire test results

The temperature distributions at different depths and their corresponding maximum temperatures obtained from the simulation of fire loading with the corrected thermal coefficient are shown in Figure 19 and Table 7.

For the RC specimen, the temperature exceeded 1200°C at 50 mm depth, indicating the occurrence of thermal spalling. The temperatures at depths of 100 mm and 150 mm were 349.45°C and 120.28°C, respectively, indicating that heat did not reach 250 mm depth. The errors between the simulation and test results at thermocouple depths of 50, 100 and 150 mm of the RC specimen were 0.5%, 9.65% and 8.89%, respectively.

For the PSC specimen, the temperature exceeded 1200°C at depths of 50 mm and 100 mm, indicating the occurrence of thermal spalling up to a depth of 100 mm, which was similar to the test result. More specifically, the temperature increased to 1200°C at 100 mm depth within 5 min after the start of fire loading. The temperature at depths of 150 mm and 250 mm was 584.58°C and 107.03°C, respectively. The errors between the simulation and test results in the thermocouples located at 50, 100, 150 and 250 mm were 1.56%, 1.49%, 4.95% and 5.57%, respectively.

For the PSRC specimen, the simulated temperature at depths of 50 mm and 100 mm was 1200°C and 297.15°C, respectively, again similar to the experimental results. However, the simulated temperatures at depths of 150 mm and 250 mm were 203.51°C and 131.96°C: 64–69°C higher than the test results. This significant error may be the result of errors accrued from implementing the temperature-dependent thermal properties of the concrete, rebars and tendons, resulting in a higher transfer of heat to these depths. Although the simulated and test temperatures at deeper depths of this specimen were dissimilar, the temperatures at depths near the fire-loaded surface were in good agreement. Since blast fire loading in PSRC members was found to be most critical at regions near the fire-loaded

surface, the simulation tool for fire- loading was considered sufficiently calibrated.

6.   Conclusions

The structural performance and failure behaviour of unbonded bi-directional PSC panels (with and without rebars) and RC panels under fire loading were evaluated. The following conclusions were drawn from this study.

(*a*) Test data on crack patterns, temperature measurement and PS force loss were obtained from fire tests. For the PSRC specimen, the combination of steel rebars and PS tendons resulted in more cracks in the specimen, which acted as pathways to release vapour gas during the fire loading.
(*b*) Thermal spalling was much larger in the PSC and PSRC specimens than in the RC specimen. Furthermore, the bottom rebars of the PSC and PSRC specimens were exposed, confirming that they were directly in contact with the fire. The damage exfoliation depth of the PSC specimens was between 199 mm and 192 mm from the fire-loaded surface.
(*c*) The FE simulation program, enhanced by implementing temperature-dependent material properties at high temperatures for the concrete rebars and PS tendons produced realistic structural behaviours under fire-loading.
(*d*) The results of simulations confirmed that the temperature distributions over time in all the specimens were quite similar. Although a temperature increase with heating time at a particular section in the RC specimen was not observed, its heat transfer was similar to that in the PSC and PSRC specimens.

Acknowledgements

REFERENCES

AAFNDSWA (Departments of the Army, Air Force, Navy and the Defense Special Weapons Agency) (1997) TM5-855-1/AFPAM32-1147/NAVFACP-1080/DAHSCWEMAN-97: Design and analysis of hardened structures to conventional weapons effects. AAFNDSWA, Washington, DC, USA.

ASME (American Society of Mechanical Engineers) (2010) *Boiler and Pressure Vessel Code III: Division 2, Code for Concrete Containments.* ASME, New York, NY, USA.

Anderberg Y (1997) Spalling phenomena of HPC of OC. In *Proceedings of International Workshop on Fire Performance of High-Strength Concrete* (Anderberg Y (ed.)). NIST, Gaithersburg, MD, USA, NIST Special Publication 919, pp. 69–73.

Baker WE (1973) *Explosions in Air.* Wilfred Baker Engineering, San Antonio, TX, USA.

Structures and Buildings
Volume 174 Issue 9

Fire resistance of bi-directionally
prestressed concrete under extreme
fire loading
Choi, Yang, Choi, Yi and Kim

BSI (1987) BS 476: Fire tests on building materials and structures –
Part 20: method for determination of the fire resistance of
elements of construction (general principles). BSI, London, UK.

BSI (2004) BS EN 1992-1-1:2004: Eurocode 2: Design of concrete
structures. General rules and rules for buildings. BSI, London, UK.

Chang SH, Choi SW, Kwon JW and Bae GJ (2006) Evaluation of
fire-induced damage to structural members in tunnels. *Journal of
the Korean Society of Civil Engineers* **26(3C)**; 219–228.

Choi SJ, Lee SW and Kim JHJ (2017) Impact or blast induced fire
simulation of bi-directional PSC panel considering concrete
confinement and spalling effect. *Engineering Structures* **149**:
113–130.

Choi SW (2013) *Estimation of Convective Heat Transfer Coefficient for
Fire-Damaged Concrete Tunnel Lining Using Model Fire Tests and
Finite Element Elimination Approach*. PhD thesis, Yonsei
University, Seoul, Korea.

DIN (Deutsches Institut für Normung) (1998) DIN 4102-1: Fire behavior
of building materials and elements – classification of building
materials – requirements and testing. DIN, Berlin, Germany.

Gustaferro AH and Selvaggio SL (1967) Fire endurance of simply
supported prestressed concrete slabs. *Journal of the Prestressed
Concrete Institute* **12(1)**: 37–52.

Ha JH, Yi NH, Kim SB, Choi JK and Kim JHJ (2010) Experimental study
on blast resistance improvement of RC panels by FRP retrofitting.
Journal of the Korea Concrete Institute **22(1)**: 93–102.

Hammer TA (1995) *High Strength Concrete Phase 3: Report 6.2.
Spalling Reduction Through Material Design*. Foundation for
Scientific and Industrial Research at the Norwegian Institute of
Technology, Trondheim, Norway.

Han LH, Tan QH and Song TY (2015) Fire performance of steel
reinforced concrete columns. *Journal of Structural Engineering,
ASCE* **141(4)**: 04014128(1-10).

Hertz K (1991) Investigations on silica fume concrete at elevated
temperatures. *Proceedings of the ACI 1991 Spring Convention,
Boston, MA, USA*.

Huo J, Zheng Q and Chen B (2009) Tests on impact behaviour of
micro-concrete-filled steel tubes at elevated temperatures up to
400°C. *Materials and Structures* **42**: 1325–1334.

Hyde DW (1992) *Fundamental of Protective Design for Conventional
Weapons, CONWEP (Conventional Weapons Effects)*. United
States Army Waterway Experiment Station, Vicksburg, MS, USA,
TM5-8511-1.

ISO (International Standards Organization) (1980) ISO 834: Fire
resistance tests – elements of building construction. ISO, Geneva,
Switzerland.

ITA (International Tunneling Association) (2004) *Guidelines for
Structural Fire Resistance for Road Tunnels*. ITA, Châtelaine,
Switzerland.

JCI (Japan Concrete Institute) (2002) *Fire Safety Research Committee for
Concrete Structures Report*. Japan Conc-Rito Institute of
Technology, Tokyo, Japan (in Japanese).

Kakogiannis D, Pascualena F, Reymen B et al. (2013) Blast performance
of reinforced concrete hollow core slabs in combination with fire:
numerical and experimental assessment. *Fire Safety Journal*
57: 69–82.

Kalifa P, Menneteau FD and Quenard D (2000) Spalling and pore
pressure in HPC at high temperatures. *Cement and Concrete
Research* **30(12)**: 1915–1927.

Kang JY, Yoon HA, Kim WS et al. (2016) Effect of wall thickness
in thermal behaviors of RC walls under fire conditions.
International Journal of Concrete Structures and Materials
10(3): S19–S31.

KSA (Korean Standards Association) (1999) *KS F 2257-1:
Methods of fire-resistant testing for structural element –
general requirements*. Korean Industrial Standards, Seoul,
South Korea.

Menzel CA (1943) Test of the fire resistance and thermal
properties of solid concrete slabs and their significance.
Proceedings of the American Society for Testing and Materials
43: 1099–1153.

SA (Standards Australia) (2005) AS1530: Method for fire tests on
building materials, components and structures, Part 4: fire-
resistance test of elements of construction. Standards Australia,
Sydney, Australia.

Schmeider U (1986) *Properties of Material at High Temperatures-
Concrete*, 2nd edn. Gesamthochsch.-Bibliothek, Gesamthochule
Kassel, Germany, RILEM Report.

Shin SW, Kwon YJ, Kim WJ et al. (2008) Fire safety design guidelines of
high strength concrete structures. *Architectural Institute of Korea*
1–50.

Won JP, Choi SW, Park CG and Park HK (2006) Temperature distribution
of wet-mixed high strength sprayed polymer mortar for fire
resistance of tunnel. *Journal of the Korean Society of Civil
Engineers* **26(4C)**: 283–290.

How can you contribute?

To discuss this paper, please email up to 500 words to the
editor at journals@ice.org.uk. Your contribution will be
forwarded to the author(s) for a reply and, if considered
appropriate by the editorial board, it will be published as
discussion in a future issue of the journal.

Proceedings journals rely entirely on contributions from the
civil engineering profession (and allied disciplines).
Information about how to submit your paper online
is available at www.icevirtuallibrary.com/page/authors,
where you will also find detailed author guidelines.